

Article

Advanced Control Strategies for Securing UAV Systems: A Cyber-Physical Approach

Mohammad Sadeq Ale Isaac ^{1,2,†}, Pablo Flores Peña ^{3,4,†,‡}, Daniela Gîfu ^{5,†} and Ahmed Refaat Ragab ^{3,4,6,*,†,‡}

¹ Computer Vision and Aerial Robotics Group, Centre for Automation and Robotics (C.A.R.), Universidad Politécnica de Madrid (U.P.M.-CSIC), 28006 Madrid, Spain; mo.aleisaackhoueini@upm.es

² Wake Engineering Company, 28906 Madrid, Spain

³ Department of Electrical Engineering, University Carlos III of Madrid, 28919 Madrid, Spain; pablo.flores@drone-hopper.com

⁴ Drone-Hopper Company, 28919 Madrid, Spain

⁵ Institute of Computer Science, Romanian Academy–Iași Branch, Codrescu 2, 700481 Iasi, Romania; daniela.gifu@iit.academiaromana-is.ro

⁶ Department of Network, Faculty of Information Systems and Computer Science, October 6 University, Giza 12511, Egypt

* Correspondence: ahmed.refaat.csis@o6u.edu.eg or a.refaat@drone-hopper.com

† These authors contributed equally to this work.

‡ Current address: Drone Hopper Research Center, Calle Mahón 8, 28290 Las Rozas de Madrid, Spain.



Citation: Ale Isaac, M.S.; Flores Peña, P.; Gîfu, D.; Ragab, A.R. Advanced Control Strategies for Securing UAV Systems: A Cyber-Physical Approach. *Appl. Syst. Innov.* **2024**, *7*, 83. <https://doi.org/10.3390/asi7050083>

Academic Editor: Igor Korobichuk

Received: 28 July 2024

Revised: 27 August 2024

Accepted: 2 September 2024

Published: 6 September 2024



Copyright: © 2024 by the authors. Published by MDPI on behalf of the International Institute of Knowledge Innovation and Invention. Licensee MDPI, Basel, Switzerland. This article is an open access article distributed under the terms and conditions of the Creative Commons Attribution (CC BY) license (<https://creativecommons.org/licenses/by/4.0/>).

1. Introduction

Unmanned aerial vehicles (UAVs) have become increasingly integral to various domains due to their versatility and cost-effectiveness, including commercial, military, and environmental applications. However, this widespread adoption has also exposed UAVs to a myriad of security threats that can compromise their functionality and safety. As the Federal Aviation Administration (FAA) projects a significant increase in commercial UAVs by 2025 [1], advanced AI-powered cybersecurity systems, like those offered by SkyGrid, provide dynamic protection through machine-learning algorithms, enhancing defense against both known and emerging threats [2]. By adopting these multi-layered security strategies, organizations can safeguard their UAV operations against the evolving landscape of cyber threats.

As UAV technology advances, their integration into ad-hoc networks like the flying ad-hoc network (FANET) is becoming increasingly viable, significantly enhancing their operational capabilities in both commercial and military domains such as logistics and surveillance [3]. However, the openness and reliance on unsecured communication protocols in FANETs increase their vulnerability to cyber-threats, including data interception, unauthorized control, and denial of service attacks. These growing threats underscore the urgent need for robust cybersecurity measures within UAV communication frameworks. Additionally, as UAVs become more prevalent across various sectors, including both legal and illicit activities, the need for advanced forensic capabilities to investigate incidents effectively becomes critical [4]. The rapid pace of technological advancement and the complexity of UAV operational environments necessitate updated protocols and regulatory frameworks to ensure security and reliability. The integration of civilian drones into everyday activities further amplifies these risks, particularly given their dependence on wireless communication and remote control systems [5]. This evolving threat landscape highlights the need for comprehensive security protocols to protect UAVs from cyberattacks and ensure their safe operation in increasingly complex environments.

Additionally, the cybersecurity vulnerabilities of UAV systems have become increasingly critical. UAVs are particularly susceptible to cyberattacks because they rely on wireless communications and remote operations, exposing them to risks such as interception, spoofing, and hijacking [6]. These vulnerabilities can lead to severe consequences, including data theft, operational disruptions, and physical damages [7]. To mitigate these risks, organizations need to implement robust security measures. These measures should include the establishment of drone detection and response procedures, the utilization of counter-UAS technologies, and the adoption of comprehensive cybersecurity solutions [8].

Meanwhile, Refs. [9–15], and other related survey works, provide a thorough overview of UAV technologies, architectures, and the security threats they face, significant strides have been made in identifying and categorizing the multifaceted security challenges across hardware, software, communication, and sensor domains. Ref. [9] focuses on a comprehensive approach to threat modeling and security assessments, yet it lacks extensive real-world validation. Ref. [10] offers an in-depth classification of vulnerabilities and countermeasures but is limited by a theoretical scope, providing little insight into practical implementations. Ref. [11] emphasizes the integration of advanced navigation algorithms and AI for UAV surveillance, though it falls short in addressing real-world adaptability. Similarly, Ref. [15] delivers a robust taxonomy of cybersecurity threats and defense mechanisms but does not thoroughly test these in dynamic environments. Additionally, Refs. [12,13] explore emerging defense technologies and AI-based security enhancements, yet they too are constrained by limited empirical validation. Collectively, these surveys underscore the urgent need for further empirical research and validation to ensure the practical effectiveness of proposed UAV security strategies across diverse operational scenarios.

Nonetheless, Ref. [16] highlights the latest advancements in UAV technology, focusing on enhanced detection mechanisms like radio frequency and radar-based systems alongside robust security measures such as jamming and signal redirection to protect against high-assault threats. In a similar vein, Ref. [17] reviews the security challenges facing drones, emphasizing vulnerabilities like unencrypted communication channels that expose UAVs to hacking and control takeovers. Both papers stress the need for improved detection, encryption, secure communication protocols, and advanced anomaly-detection systems to defend against cyber and physical threats. Additionally, Refs. [18,19] outline the increasing complexity of these threats, advocating for the integration of emerging technologies like mmWave, massive MIMO, cognitive radio, machine learning, and the blockchain to enhance UAV security. The reviews collectively underscore the critical importance of comprehensive cybersecurity frameworks in maintaining the integrity and safety of UAV operations.

Given the dual threats faced by UAV systems, including physical attacks like interception and sabotage, as well as cyber-threats such as hacking and data breaches, a combined cyber-physical security approach is essential. Advanced non-linear control strategies, like

sliding mode control, adaptive control, and robust control, are critical in ensuring responsive and adaptable UAV operations. In line with this, Ref. [20] presents an approach to enhancing UAV safety by detecting and compensating for attacks on flight trajectories, particularly when trajectory data are compromised. The study introduces attack detection and compensation mechanisms, including an attack observer (AO) and learning observer (LO), which effectively distinguish between genuine disturbances and malicious attacks, as demonstrated through simulations and experimental tests.

Focusing on sliding mode control (SMC), its inherent robustness against disturbances and its ability to maintain performance under uncertain conditions make it an ideal choice for dealing with unpredictable security challenges in UAV operations. To address these challenges, the author's previous works have concentrated on developing robust and adaptive control methods for multi-ducted fan platforms aimed at maintaining system stability during payload release and firefighting applications. Specifically, model reference adaptive control (MRAC) was employed to counteract internal uncertainties, such as changes in weight, while sliding mode control (SMC) algorithms were designed to mitigate the effects of external disturbances [21–24].

Nevertheless, Ref. [25] addresses the security and formation tracking of multi-UAV systems under replay attacks by introducing an observer-based event-triggered sliding mode control approach, which optimizes communication-based on attack severity to reduce data transmission and energy consumption while maintaining performance. Similarly, Ref. [26] presents a novel strategy for detecting and isolating cyber-attacks on quadrotor UAVs, using modified sliding innovation sequences (MSIS) combined with an extended Kalman filter (EKF) to enhance robustness against various cyber-threats, including false data injection and denial-of-service attacks, with demonstrated effectiveness in simulations. Additionally, Ref. [27] proposes a sliding mode control approach for multi-UAV air combat management, integrating a threat assessment model and matrix game theory for strategic target allocation, supported by a social behavioral-based control for managing UAV swarm motion, which has been validated through simulation tests.

Meanwhile, Ref. [28] presents an advanced control methodology for fixed-wing UAVs, introducing an adaptive backstepping sliding mode control technique that effectively manages altitude, attitude, and velocity despite non-linearity and multi-variable coupling, with real-time adjustments for uncertainties validated through extensive numerical simulations. Similarly, Ref. [29] focuses on a robust control algorithm for quadrotor UAVs, utilizing fixed-time sliding mode control (FTSMC) based on Lyapunov theory to ensure stability and precise trajectory tracking despite disturbances. This study compares FTSMC with non-singular terminal sliding mode control (NTSMC), highlighting FTSMC's superior efficiency in reducing disturbances, making it well-suited for dynamic operational environments.

Consequently, this paper focuses on developing and implementing a novel sliding mode control (SMC)-based framework specifically designed to enhance UAV security by dynamically responding to both cyber and physical threats. Unlike previous studies that have typically addressed either cyber or physical threats in isolation, this work integrates both into a unified control strategy, thereby improving UAV resilience and operational integrity in hostile environments. The proposed framework not only leverages the robustness of SMC against external disturbances but also introduces adaptive mechanisms that allow the UAV to respond in real-time to evolving threats, which represents a significant advancement over existing methods that often lack such adaptability and comprehensive threat-mitigation capabilities.

This paper is organized into four sections: Section 2 discusses the proposed control methodology and denotes the simulation procedure, Section 3 shows the results, and Section 4 concludes the paper.

2. Advanced Sliding Mode Control Framework for UAV Security

This section presents an advanced sliding mode control (SMC) framework tailored for enhancing the security of unmanned aerial vehicle (UAV) systems, specifically focusing on helicopter dynamics. The proposed methodology integrates adaptive and fault-tolerant mechanisms to ensure robust and resilient UAV operations against both physical and cyber threats.

2.1. Helicopter Dynamics

A set of non-linear differential equations typically represents the dynamic model of a helicopter, which is defined with respect to two primary coordinate systems: the inertial frame and the body frame, as depicted in Figure 1.

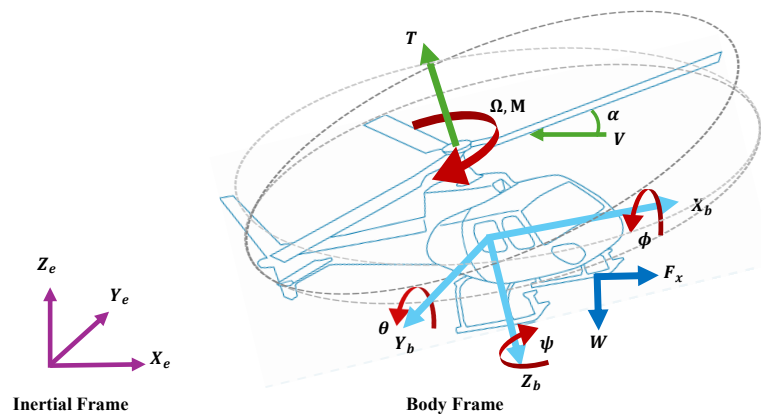


Figure 1. The inertial frame vs. body frame of the helicopter. Different colors are used for a clearer distinction between the components of each frame.

- **Inertial Frame ($\mathbf{X}_e, \mathbf{Y}_e, \mathbf{Z}_e$):** The inertial frame is a fixed coordinate system that serves as a reference for the helicopter's position and orientation in space. The axes \mathbf{X}_e , \mathbf{Y}_e , and \mathbf{Z}_e are typically aligned with the north-east-down (NED) or Earth-centered Earth-fixed (ECEF) directions, providing a global reference for the helicopter's movement. Forces such as the gravitational force \mathbf{W} act in this frame, influencing the helicopter's position and orientation. Also, the velocity vector \mathbf{V} represents the helicopter's speed and direction of movement relative to the inertial frame.
- **Body Frame ($\mathbf{X}_b, \mathbf{Y}_b, \mathbf{Z}_b$):** The body frame is a moving coordinate system that is fixed to the helicopter. The axes \mathbf{X}_b , \mathbf{Y}_b , and \mathbf{Z}_b are aligned with the helicopter's forward, right, and downward directions, respectively. This frame is used to describe the helicopter's dynamics relative to its own structure. The forces and moments, such as thrust (\mathbf{T}), angular velocities ($\boldsymbol{\Omega}$), and moments (\mathbf{M}), are represented in this frame, influencing the helicopter's movement and stability. The thrust vector \mathbf{T} generated by the helicopter's propeller and the resulting moments \mathbf{M} around the helicopter's center of mass are critical for controlling the helicopter's movement and stability in three-dimensional space. The figure also introduces key aerodynamic elements such as the angle of attack (α), which affects the lift and drag forces on the helicopter, and the resultant aerodynamic force components along the \mathbf{X}_b , \mathbf{Y}_b , and \mathbf{Z}_b axes. Additionally, the rotational angles (roll ϕ , pitch θ , and yaw ψ) define the orientation of the helicopter relative to the Body Frame.

In this dynamic model, the state vector \mathbf{x} includes positions, velocities, attitudes, and angular rates, all of which are expressed in the body frame. Control inputs \mathbf{u} , such as the collective pitch, longitudinal cyclic pitch, lateral cyclic pitch, and tail rotor pitch, are also defined relative to the body frame. The helicopter's dynamics are influenced by forces and moments that are calculated in the body frame but can be transformed into the inertial frame for a global perspective on the helicopter's motion. The state vector \mathbf{x} for a

helicopter includes positions, velocities, attitudes, and angular rates. The control inputs \mathbf{u} include the collective pitch, longitudinal cyclic pitch, lateral cyclic pitch, and tail rotor pitch. The helicopter's dynamics can be described as:

$$\dot{\mathbf{x}} = \mathbf{f}(\mathbf{x}) + \mathbf{B}(\mathbf{x})\mathbf{u} + \mathbf{d}(t), \quad (1)$$

where $\mathbf{x} = [\phi, \theta, \psi, p, q, r, u, v, w, x, y, z]^T$ represents the state vector; ϕ, θ, ψ are the roll, pitch, and yaw angles; p, q, r are the angular rates; u, v, w are the velocities in the body frame; x, y, z are the positions in the inertial frame; $\mathbf{B}(\mathbf{x})$ is the control effectiveness matrix, reflecting the non-linear dynamics of the system and mapping the control inputs \mathbf{u} to the changes in the state vector \mathbf{x} ; $\mathbf{u} = [u_1, u_2, u_3, u_4]^T$ are the control inputs; and $\mathbf{d}(t)$ represents external disturbances and uncertainties.

In Equation (1), the control objective is to drive the state \mathbf{x} to follow a desired trajectory \mathbf{x}_d .

2.1.1. Translational Dynamics

Newton's second law governs the translational motion of the helicopter:

$$m\ddot{\mathbf{x}} = \mathbf{F}, \quad (2)$$

where m is the mass of the helicopter; $\ddot{\mathbf{x}} = [\ddot{x}, \ddot{y}, \ddot{z}]^T$ represents the acceleration vector in the inertial frame; and $\mathbf{F} = [F_x, F_y, F_z]^T$ represents the total force vector acting on the helicopter.

The forces acting on the helicopter include aerodynamic forces, gravitational force, and control inputs. The gravitational force is given by:

$$\mathbf{F}_g = [0, 0, -mg]^T, \quad (3)$$

where g is the acceleration due to gravity.

2.1.2. Rotational Dynamics

The rotational dynamics of the helicopter can be described using Euler's rotational equations:

$$\mathbf{J}\dot{\boldsymbol{\omega}} = \boldsymbol{\tau} - \boldsymbol{\omega} \times (\mathbf{J}\boldsymbol{\omega}), \quad (4)$$

where \mathbf{J} is the inertia matrix of the helicopter; $\boldsymbol{\omega} = [p, q, r]^T$ represents the angular velocity vector in the body frame; and $\boldsymbol{\tau} = [\tau_x, \tau_y, \tau_z]^T$ represents the total torque vector acting on the helicopter.

Rotor Dynamics and Flapping Motion

The rotor dynamics, particularly the flapping motion, significantly influence the stability and control of the helicopter. The blade flapping motion is described by the flapping angle β , influenced by aerodynamic forces, inertial forces, and control inputs. The flapping motion is modeled as follows:

$$\ddot{\beta} + \omega_\beta^2 \beta = 0, \quad (5)$$

where ω_β is the natural frequency of the flap. The blade response considering aerodynamic forces can be represented as:

$$\ddot{\beta} + 2\zeta\omega_\beta\dot{\beta} + \omega_\beta^2\beta = M_\beta, \quad (6)$$

where M_β is the aerodynamic flap moment, ζ is the damping ratio, and ω_β is the flapping frequency.

Aerodynamic Damping and Control Inputs

The control inputs, including the longitudinal and lateral cyclic pitches and the collective pitch, play crucial roles in the helicopter's rotational dynamics. These inputs modify the orientation of the thrust vector, impacting the helicopter's roll, pitch, and yaw motions. The dynamics are captured by [30]:

$$\dot{\theta}_a = -\frac{1}{\tau_m}\theta_a + \frac{k_\beta}{2\Omega I_\beta}\theta_b + \frac{1}{\tau_m}\theta_a + d_a, \quad (7)$$

$$\dot{\theta}_b = -\frac{1}{\tau_m}\theta_b + \frac{k_\beta}{2\Omega I_\beta}\theta_a + \frac{1}{\tau_m}\theta_b + d_b, \quad (8)$$

where θ_a and θ_b are the longitudinal and lateral cyclic inputs, k_β is the blade root stiffness, I_β is the blade moment of inertia about the flap hinge, Ω is the rotor angular speed, and τ_m is the rotor time constant. The terms d_a and d_b represent unknown disturbances.

Rotor Dynamics and Flapping Motion

The rotor dynamics are crucial in determining the helicopter's behavior. The main rotor blades are not rigid and exhibit flapping motion, which can be represented by the flapping angles a and b for longitudinal and lateral directions, respectively. The equations can describe these dynamics:

$$\begin{aligned} \dot{a} &= \gamma_m \Omega \left(\frac{-4k_\beta}{I_\beta \Omega^2} - 8 \right) a - p + \gamma_m \Omega \left(\frac{-\gamma_m}{\gamma_m^2 + 64} \right) B_m \\ \dot{b} &= \gamma_m \Omega \left(\frac{\gamma_m}{\gamma_m^2 + 64} \right) b - q + \gamma_m \Omega \left(\frac{8}{\gamma_m^2 + 64} \right) A_m, \end{aligned} \quad (9)$$

where γ_m is the Lock number, Ω is the rotor angular velocity, I_β is the blade moment of inertia, k_β is the blade stiffness coefficient, and A_m, B_m are cyclic pitch angles [31].

Forces and Moments

The dominant forces and moments on the helicopter come from the main rotor and can be expressed as follows:

$$\begin{aligned} F_x &= -T \sin a, \\ F_y &= T \sin b, \\ F_z &= -T \cos a \cos b, \\ M_x &= (k_\beta + TH_{mr})b, \\ M_y &= (k_\beta + TH_{mr})a, \end{aligned} \quad (10)$$

where T is the thrust, H_{mr} is the main rotor height, and (a, b) are the flapping angles.

Considerations for Control Design

The inclusion of rotor dynamics and actuator dynamics, as well as aerodynamic damping, is essential for accurate modeling and control design. These dynamics can significantly affect the helicopter's response to control inputs, making it critical to incorporate them into the control strategy to ensure stability and performance.

2.2. Enhanced Sliding Mode Control Design for Helicopter Attitude

2.2.1. Sliding Surface Definition

The sliding surfaces $S_\phi(x)$, $S_\theta(x)$, and $S_\psi(x)$ for roll, pitch, and yaw controls are defined as:

$$\begin{aligned} S_\phi(x) &= \dot{e}_\phi + \lambda_\phi e_\phi, \\ S_\theta(x) &= \dot{e}_\theta + \lambda_\theta e_\theta, \\ S_\psi(x) &= \dot{e}_\psi + \lambda_\psi e_\psi, \end{aligned} \quad (11)$$

where $e_\phi = \phi - \phi_d$, $e_\theta = \theta - \theta_d$ and $e_\psi = \psi - \psi_d$ are the tracking errors for roll, pitch, and yaw angles, respectively, and λ_ϕ , λ_θ , and λ_ψ are positive definite matrices that shape the dynamics of the sliding surfaces.

2.2.2. Control Law

The control input u is designed to drive the sliding surfaces $S_\phi(x)$, $S_\theta(x)$, and $S_\psi(x)$ to zero in finite time. It consists of an equivalent control u_{eq} and a switching control u_s :

$$u = u_{eq} + u_s \quad (12)$$

Equivalent Control

The equivalent control u_{eq} compensates for the system's nominal dynamics:

$$\begin{aligned} u_{eq,\phi} &= -B_\phi(x)^{-1}(f_\phi(x) + \dot{\phi}_d - \lambda_\phi e_\phi), \\ u_{eq,\theta} &= -B_\theta(x)^{-1}(f_\theta(x) + \dot{\theta}_d - \lambda_\theta e_\theta), \\ u_{eq,\psi} &= -B_\psi(x)^{-1}(f_\psi(x) + \dot{\psi}_d - \lambda_\psi e_\psi) \end{aligned} \quad (13)$$

Switching Control

The switching control u_s handles uncertainties and disturbances:

$$\begin{aligned} u_{s,\phi} &= -K_\phi \tanh(S_\phi(x)), \\ u_{s,\theta} &= -K_\theta \tanh(S_\theta(x)), \\ u_{s,\psi} &= -K_\psi \tanh(S_\psi(x)), \end{aligned} \quad (14)$$

where K_ϕ , K_θ , and K_ψ are positive gain matrices.

By replacing the sign function $sgn()$ with the hyperbolic tangent function $tanh()$, the control law transitions more smoothly as the system approaches the sliding surface. While the sign function introduces a sharp switch, leading to potential chattering near the sliding surface, the hyperbolic tangent function provides a continuous and differentiable approximation, reducing chattering and ensuring that the system reaches the sliding surface more gradually. This smooth transition helps improve system stability and performance, particularly in the presence of high-frequency disturbances or model uncertainties.

2.3. Adaptive and Fault-Tolerant Mechanisms

To enhance robustness, adaptive and fault-tolerant mechanisms are integrated:

2.3.1. Adaptive Gain Adjustment

The switching gain K is dynamically adjusted based on the sliding surface magnitude:

$$K(t) = K_0 + \gamma \|S(x)\|, \quad (15)$$

where K_0 is the baseline gain and γ is the adaptation rate parameter.

2.3.2. Fault-Tolerant Control

To enhance the robustness and reliability of the helicopter control system, particularly in the presence of actuator/sensor faults or external disturbances, the fault-tolerant control (FTC) strategies are incorporated into the existing SMC framework. These strategies are designed to detect, isolate, and compensate for faults, ensuring the helicopter maintains stable operation when the control system reconfigures itself by:

- Fault detection and isolation (FDI): Implementing FDI algorithms to detect and isolate faults, ensuring system integrity.
- Reconfiguring control parameters: Adjusting λ and other control parameters to compensate for faults.

- Utilizing redundancy: Leveraging redundant actuators and sensors to maintain control despite component failures.

These enhancements ensure the SMC framework can robustly handle unexpected disturbances and maintain stable control of the helicopter's attitude, which are explained next.

2.3.3. Fault Detection and Isolation (FDI)

FDI is a critical component of FTC. The FDI system monitors the helicopter's sensors and actuators, identifying discrepancies that indicate potential faults.

The residual vector $r(t)$ is calculated as:

$$r(t) = y(t) - \hat{y}(t), \quad (16)$$

where $y(t)$ is the actual output from the sensors, and $\hat{y}(t)$ is the estimated output based on the nominal model of the system.

A fault is detected if the residual exceeds a predefined threshold:

$$\|r(t)\| > \delta \Rightarrow \text{Fault detected.} \quad (17)$$

Upon detecting a fault, the FDI system isolates the faulty component and provides this information to the control system.

2.3.4. Reconfiguration of Control Parameters

Once a fault is detected and isolated, the control system adapts by reconfiguring its parameters to compensate for the fault. The control parameters λ_ϕ , λ_θ , and λ_ψ in the sliding surfaces are adjusted as follows:

$$\begin{aligned} \lambda_\phi &= \lambda_{\phi_0} + \Delta\lambda_\phi, \\ \lambda_\theta &= \lambda_{\theta_0} + \Delta\lambda_\theta, \\ \lambda_\psi &= \lambda_{\psi_0} + \Delta\lambda_\psi, \end{aligned} \quad (18)$$

where λ_{ϕ_0} , λ_{θ_0} , and λ_{ψ_0} are the nominal values of the parameters, and $\Delta\lambda_\phi$, $\Delta\lambda_\theta$, and $\Delta\lambda_\psi$ are the adjustments based on the detected fault.

These adjustments help maintain the desired system performance even in the presence of component degradation or failure.

2.3.5. Redundancy and Control Allocation

The system can also leverage redundancy by redistributing control efforts among the remaining operational actuators. Consider the control input vector u split among n actuators, with a weighting matrix W that allocates the control effort:

$$u = W \cdot u', \quad (19)$$

where u' is the original control input vector and W is a reconfiguration matrix that adjusts the distribution of control inputs based on the status of the actuators.

If an actuator fault is detected, the corresponding row in W is modified to reduce or eliminate control input to the faulty actuator, reallocating it to the operational actuators:

$$W = \begin{bmatrix} w_{11} & w_{12} & \dots & 0 & \dots & w_{1n} \\ w_{21} & w_{22} & \dots & 0 & \dots & w_{2n} \\ \vdots & \vdots & \vdots & \vdots & \vdots & \vdots \\ w_{n1} & w_{n2} & \dots & 0 & \dots & w_{nn} \end{bmatrix}, \quad (20)$$

where the zero entries correspond to the faulty actuator, effectively isolating it from the control loop.

2.3.6. Adaptive Sliding Mode Control

To further enhance fault tolerance, the control gains $K_\phi(t)$, $K_\theta(t)$, and $K_\psi(t)$ are adapted based on the sliding surface magnitude and detected faults:

$$\begin{aligned} K_\phi(t) &= K_{\phi_0} + \gamma_\phi \|S_\phi(x)\| + \alpha_\phi \Delta K_\phi, \\ K_\theta(t) &= K_{\theta_0} + \gamma_\theta \|S_\theta(x)\| + \alpha_\theta \Delta K_\theta, \\ K_\psi(t) &= K_{\psi_0} + \gamma_\psi \|S_\psi(x)\| + \alpha_\psi \Delta K_\psi, \end{aligned} \quad (21)$$

where $K_{\phi_0}, K_{\theta_0}, K_{\psi_0}$ are the baseline gains, $\gamma_\phi, \gamma_\theta, \gamma_\psi$ are the adaptation rates, and $\alpha_\phi, \alpha_\theta, \alpha_\psi$ are fault-dependent gain adjustment factors.

2.3.7. Simulation Setup

The helicopter model is subjected based on a real helicopter study case called Nuntius-02, belonging to Drone Hopper Research Center, and the details of this UAV are described in Table 1. The control system's response to these attacks is evaluated, demonstrating the robustness and adaptability of the proposed SMC framework.

Table 1. Specification of the Nuntius-02 study case.

Component	Parameter	Value	Dimension
<i>Fuselage</i>	MTOW	25	Kg
	M_{PL}	2	Kg
	Height	64.4	cm
	Length	157.6	cm
	Length	54	cm
	I_{xx}	5.43	$\text{kg}\cdot\text{m}^2$
	I_{yy}	5.30	$\text{kg}\cdot\text{m}^2$
	I_{zz}	1.36	$\text{kg}\cdot\text{m}^2$
	V_{max}	120	km/h
	V_{cruise}	90	km/h
<i>Propeller</i>	Blade number	2	—
	Blade radii	90	cm
	Blade tip Chord	15	cm
	Blade tip Angle	8	deg
	Nominal rotor rev.	1300	rpm
	Thrust factor	2.16×10^{-2}	$\text{N}\cdot\text{m}^2$
	Blade moment of inertia (I_β)	0.167	$\text{kg}\cdot\text{m}^2$
<i>Servo flap</i>	Number	3	—
	Avg. speed	0.16	$\text{s}/60^\circ$
	Input signal	50	Hz
	Rated torque	25	$\text{kg}\cdot\text{cm}$

Additionally, the following parameters and equations were used to model the dynamics and control of the Nuntius-02 helicopter.

2.4. Blade Moment of Inertia

The blade moment of inertia about the flap hinge is given by:

$$I_\beta = \frac{1}{3}mL^2 = \frac{1}{3} \times 0.5 \text{ kg} \times (1 \text{ m})^2 = 0.167 \text{ kg} \cdot \text{m}^2$$

2.5. Thrust Force

The thrust force generated by the rotor is calculated as:

$$T = C_T \cdot \rho \cdot A \cdot \Omega^2 \cdot R^2 = 0.005 \cdot 1.225 \cdot \pi \cdot (0.9)^2 \cdot (136.1)^2 \cdot (0.9)^2 = 148.56 \text{ N}$$

2.6. Rotor Flapping Motion

The flapping motion of the rotor blade is described by:

$$\beta(t) = \frac{M_\beta}{I_\beta \cdot \omega_\beta^2} = \frac{M_\beta}{0.167 \cdot 15^2} = \frac{M_\beta}{37.575}$$

2.7. Rotational Dynamics

The rotational dynamics around the helicopter's axes are expressed as:

$$\dot{\omega} = J^{-1}(\tau - \omega \times (J \cdot \omega))$$

where:

$$J = \begin{pmatrix} 5.43 & 0 & 0 \\ 0 & 5.30 & 0 \\ 0 & 0 & 1.36 \end{pmatrix} \text{ kg} \cdot \text{m}^2$$

2.8. Aerodynamic Damping

The aerodynamic damping is calculated as:

$$\zeta = \frac{C_d \cdot \rho \cdot A \cdot \Omega \cdot R}{2m} = 0.0142 \text{ s}^{-1}$$

Consequently, the following results in the next section were obtained from simulations conducted in the Gazebo environment, utilizing parameters derived from a CAD model of the Nuntius-02 helicopter described in Table 1. The simulation was performed using a controller modified version of the PX4-Autopilot, running on an Ubuntu-based platform. Key formats, such as SDF (simulation description format), were used to represent the UAV model and its physical properties accurately. This setup allowed for the precise simulation of the UAV's dynamics under various conditions, including disturbances and control strategies.

3. Results

Simulation results show that the SMC-based control system successfully maintains stability and performance in the presence of disturbances and attacks. The adaptive and fault-tolerant mechanisms effectively compensate for anomalies, ensuring resilient UAV operations.

Figure 2 illustrates the performance data of the Nuntius model helicopter controlled by the secured SMC during 45 min of flight. The results are divided into several subplots, each focusing on critical flight parameters and their respective control inputs.

- Altitude (top-left): The altitude plot displays the helicopter's desired altitude (Z_d) versus the actual altitude (Z). The SMC effectively maintains the desired altitude with minimal deviations, demonstrating its robustness in altitude control.
- Throttle (top-right): The throttle percentage plot shows the control effort required to maintain and adjust altitude. Despite some fluctuations, the throttle remains within an acceptable range, indicating the controller's efficiency in managing the helicopter's power.
- Flight trajectory (center): The 3D flight trajectory plot depicts the helicopter's path in the XY-plane over time. The trajectory is smooth and consistent, reflecting the controller's ability to guide the helicopter along a predefined path accurately.
- Roll, pitch, and yaw (bottom-left): These plots represent the helicopter's roll (ϕ), pitch (θ), and yaw (ψ) angles compared to their respective desired values. The controller maintains these angles with high precision, ensuring stable and balanced flight. The minor oscillations observed are typical in such dynamic systems and are well within acceptable limits.

- Servo flap positions (bottom-right): The positions of the roll, pitch, and yaw servo flaps are shown, indicating the control surface adjustments made to achieve the desired flight dynamics. The servo responses are rapid and precise, reflecting the controller's ability to translate control commands into physical movements effectively.

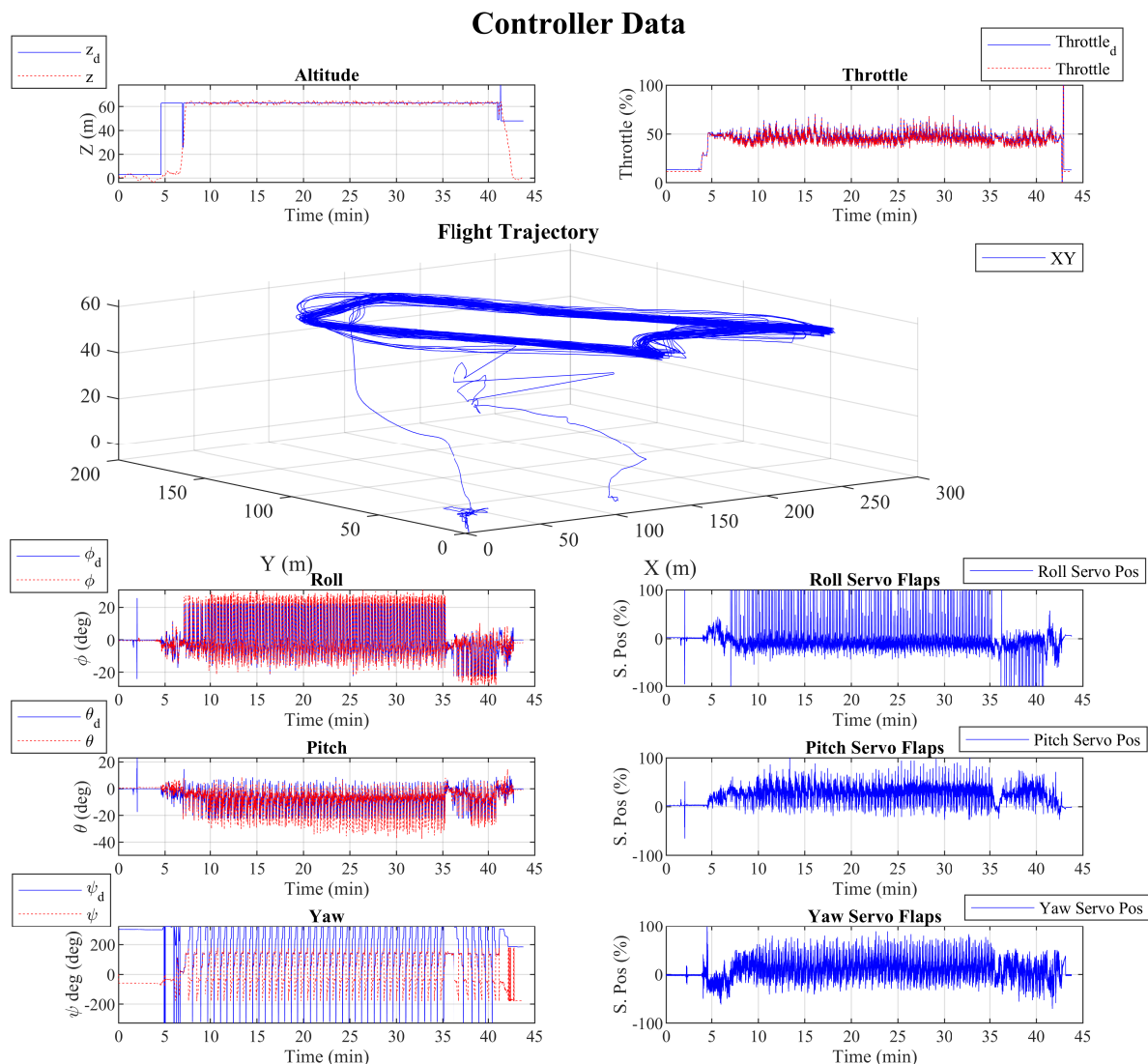


Figure 2. Performance of the helicopter's control system in the presence of the secured algorithm, highlighting various key parameters and their behavior over a 45-min flight. The subplots present altitude, throttle, flight trajectory, roll, pitch, yaw, and corresponding servo flap positions.

Figure 3 shows the second performance data of the Nuntius helicopter controlled by a secured SMC for a 45-min flight, applying random noise over the yaw angle between minutes 10 and 20. The results are divided into several subplots, each focusing on critical flight parameters and their respective control inputs.

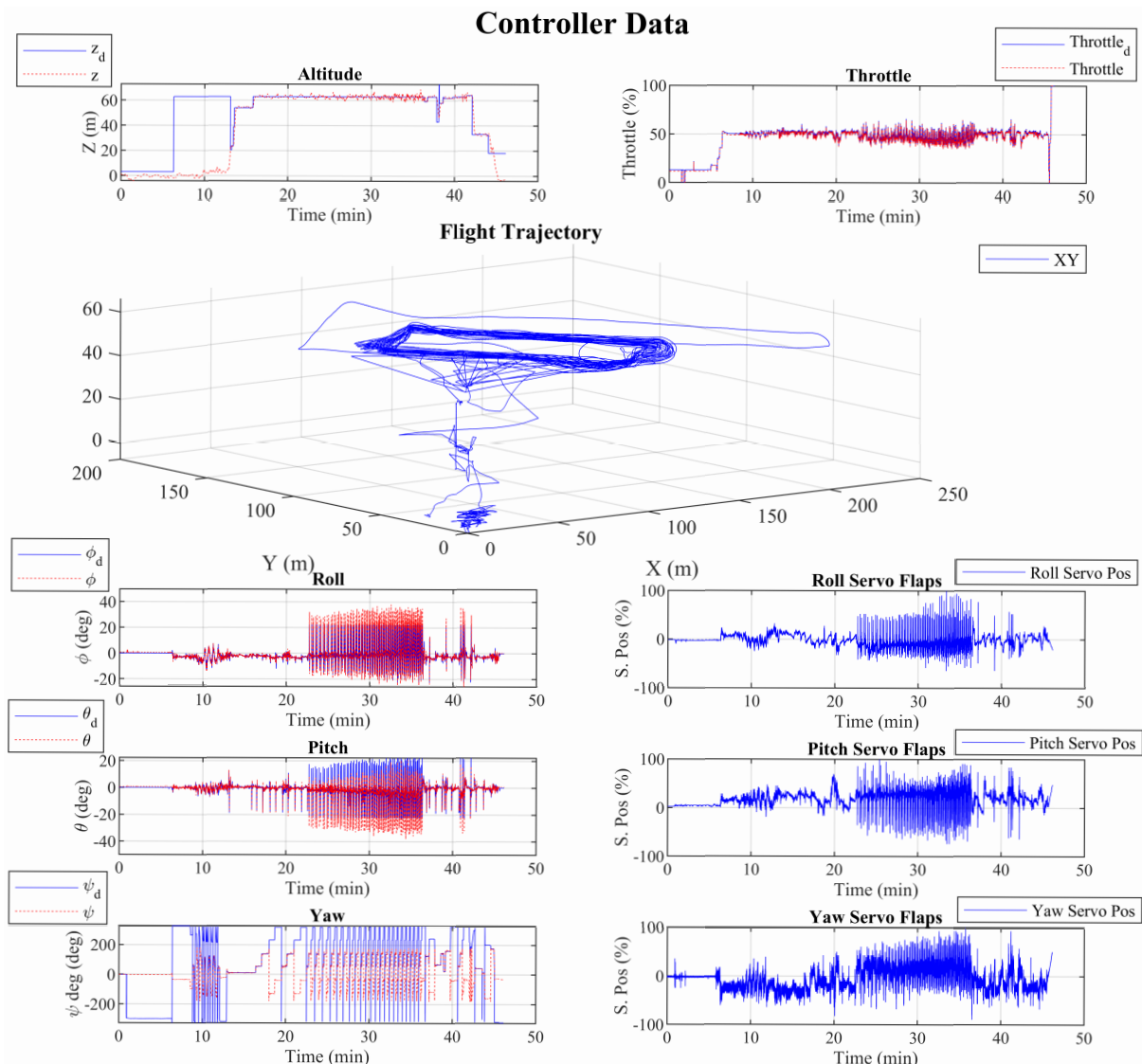


Figure 3. Performance data of the Nuntius helicopter controlled by a secured SMC during a 45-min flight with random noise applied to the yaw angle between minutes 10 and 20. The subplots display critical flight parameters and corresponding control inputs.

- Altitude (top-left): The altitude subplot demonstrates the helicopter's altitude control performance. The actual altitude closely follows the desired altitude, indicating robust altitude maintenance by the SMC. The controller's ability to handle altitude disturbances and maintain stability is evident, particularly when the yaw disturbance is applied between 10 and 20 min.
- Throttle (top-right): The throttle input percentage is plotted over time, showing how the SMC adjusts the throttle to counteract the effects of disturbances. The plot reveals that the controller modulates the throttle input smoothly, maintaining the desired flight profile despite the random noise applied to the yaw.
- Flight trajectory (center): The 3D flight trajectory plot illustrates the helicopter's path during the flight. Despite the yaw disturbances between minutes 10 and 20, the trajectory shows minimal deviation, indicating that the SMC effectively compensates for the disturbances. The SMC ensures the helicopter returns to the desired flight path, demonstrating strong resilience and disturbance rejection.
- Roll, pitch, and yaw (bottom-left):

- Roll: The roll angle plot shows the actual roll versus the desired roll angle. The SMC maintains the roll angle within acceptable bounds, even under yaw disturbances, illustrating the controller's capability to manage cross-coupled effects.
- Pitch: Similar to roll, the pitch angle plot presents the actual and desired angles. The SMC's control effectively mitigates pitch disturbances, maintaining stability and alignment with the desired pitch trajectory.
- Yaw: The yaw plot highlights the impact of the random noise applied between minutes 10 and 20. Despite the noise, the SMC manages to keep the actual yaw close to the desired yaw, showcasing the controller's robustness against yaw disturbances.
- Servo flap positions (bottom-right):
 - Roll servo flaps: This subplot displays the roll servo positions over time. The SMC adjusts the servo positions dynamically, indicating the control surface's response to counteract roll disturbances and maintain stability.
 - Pitch servo flaps: The plot shows the pitch servo positions, where the SMC adjusts the controls to correct any deviations in pitch. The control responses are smooth, reflecting the SMC's ability to handle pitch disturbances effectively.
 - Yaw servo flaps: The yaw servo positions are plotted, demonstrating the SMC's response to the induced yaw disturbances. The controller adjusts the servo positions to maintain the desired yaw, even under random noise, highlighting the system's disturbance rejection capabilities.

Figure 4 shows the third performance data of the Nuntius helicopter controlled by a secured SMC for a 30-min flight, applying assisted-manual commands after minute 20. The results are divided into several subplots, each focusing on critical flight parameters and their respective control inputs.

- Altitude (top-left): The altitude subplot shows the helicopter's altitude (red) and the desired altitude (blue). At around minute 20, the pilot reduced the throttle, resulting in a descent from 60 m to approximately 20–25 m. The secured SMC adjusted to this change, demonstrating its capability to stabilize the helicopter despite the unexpected manual input.
- Throttle (top-right): The throttle subplot indicates a noticeable reduction at minute 20, corresponding with the pilot's intervention. The controller responded by adjusting the throttle input to mitigate the descent rate and maintain control over the aircraft's altitude.
- Flight trajectory (center): The 3D plot of the flight trajectory illustrates the helicopter's path, with notable changes in altitude and horizontal positioning after minute 20. Despite the pilot's manual commands, the SMC maintained a controlled descent and kept the helicopter within a manageable flight envelope.
- Roll, pitch, and yaw (bottom-left):
 - Roll: The roll angle plot shows increased activity after minute 20, where the pilot's manual inputs caused fluctuations in the roll angle. The SMC compensated by adjusting the roll control inputs to stabilize the helicopter.
 - Pitch: Similar to roll, the pitch angle plot displays increased fluctuations post minute 20 due to manual inputs. The controller's corrective actions are evident, as it worked to maintain the desired pitch despite the disturbances.
 - Yaw: The yaw plot demonstrates the manual yaw adjustments made by the pilot. The SMC managed to control the yaw movements, keeping them within acceptable limits and preventing excessive deviation from the desired trajectory.
- Servo flap positions (bottom-right):
 - Roll servo flaps: The roll servo positions show significant activity as the controller worked to counteract the manual roll inputs and maintain stability.

- Pitch servo flaps: The pitch servo positions also reflect the controller's adjustments to the manual pitch inputs, highlighting the SMC's ability to manage unexpected control inputs.
- Yaw servo flaps: The yaw servo positions illustrate the controller's response to manual yaw inputs, ensuring that the helicopter remained under control despite the disturbances.

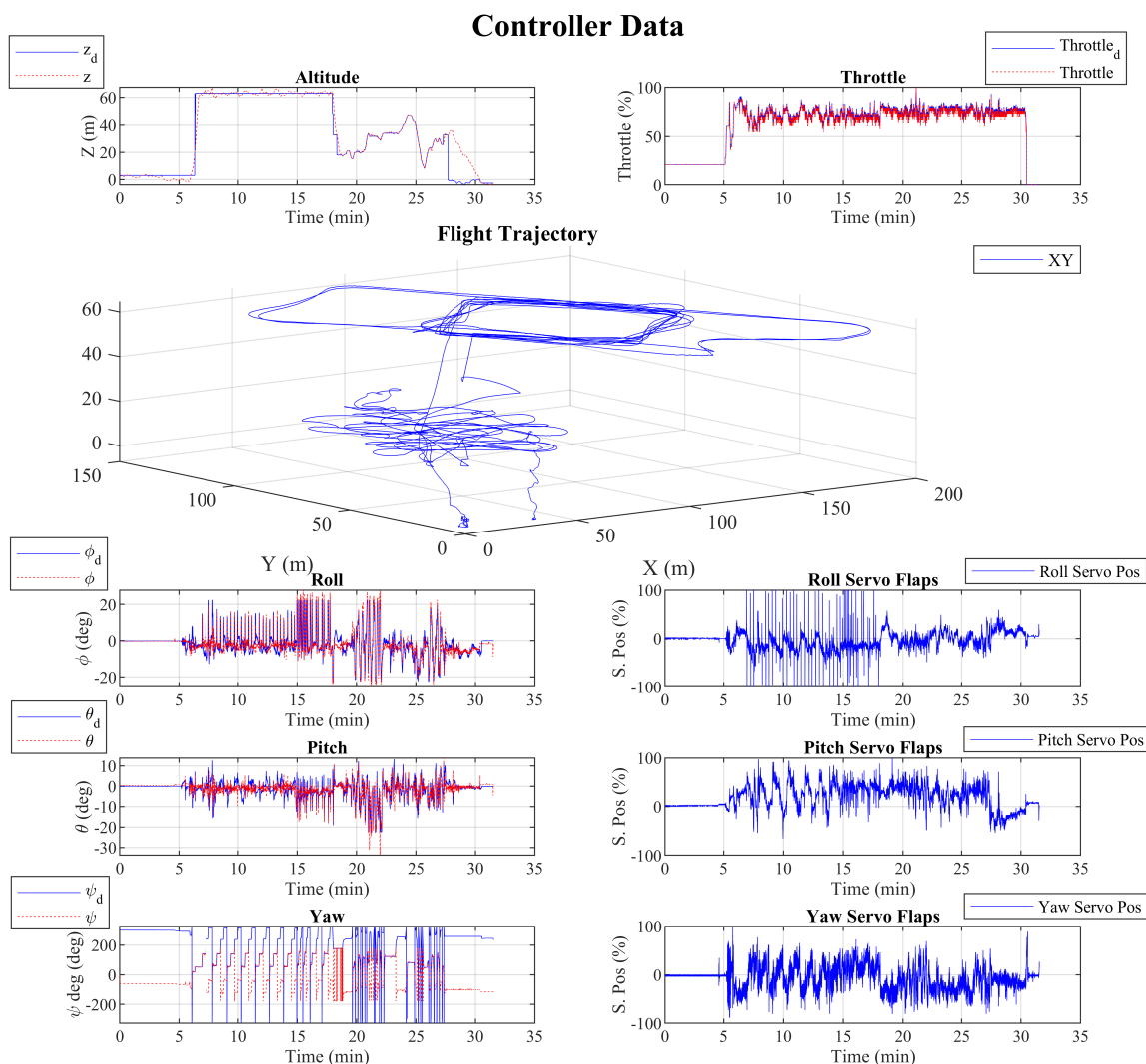


Figure 4. Performance data of the Nuntius helicopter controlled by a secured SMC during a 35-min flight. The pilot began sending assisted-manual commands at around minute 20, starting with a throttle reduction. The data highlight the controller's compensation for these inputs, maintaining stability despite the manual interventions.

Figure 5 shows the third performance data of the Nuntius helicopter controlled by a secured SMC for a 45-min flight, changing the route direction at around minute 30. The results are divided into several subplots, each focusing on critical flight parameters and their respective control inputs.

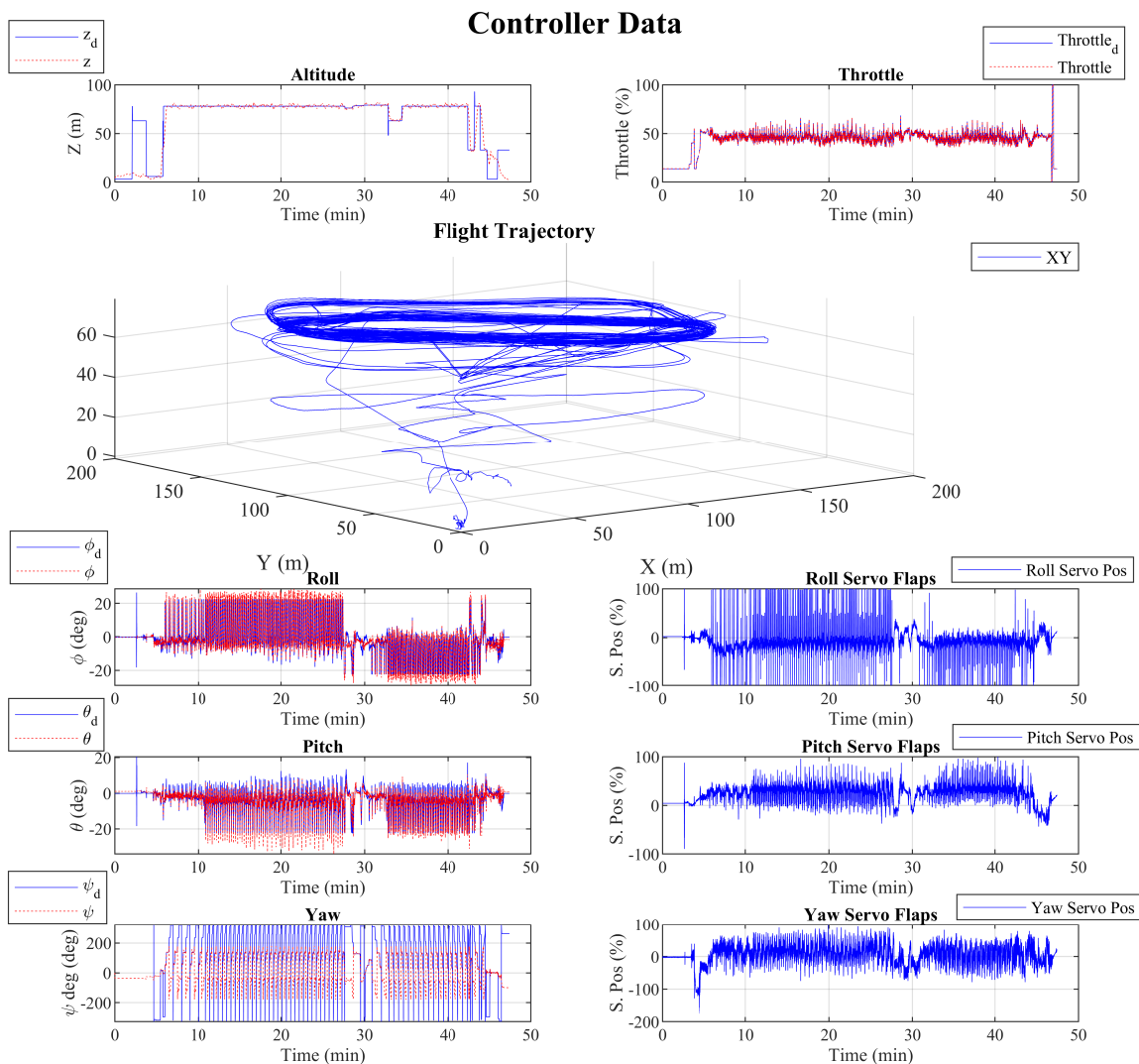


Figure 5. Performance data of the Nuntius helicopter controlled by a secured SMC during a 45-min flight. At around minute 30, a changing direction was applied to the roll loop to test the attitude control performance. The figure showcases the helicopter’s response to this input across various flight parameters.

- Altitude (top-left): The altitude subplot presents the actual altitude (in red) and the desired altitude (in blue). Around minute 30, despite the roll direction change, the altitude remains relatively stable, indicating effective control by the SMC in maintaining vertical position.
- Throttle (top-right): The throttle input is shown to vary as the helicopter adjusts to the changing roll commands around minute 30. The controller modulates the throttle to manage power distribution, ensuring continued control over the altitude and horizontal motion.
- Flight trajectory (center): The 3D flight trajectory illustrates the helicopter’s path, highlighting the region around minute 30 where the roll direction change was applied. The trajectory shows a consistent pattern with minimal deviation, indicating that the SMC maintained stability and effectively managed the attitude adjustment.
- Roll, pitch, and yaw (bottom-left):
 - Roll: The roll angle subplot captures the actual (red) and desired (blue) roll angles, particularly focusing on the period around minute 30. The data show an increase

- in roll activity, demonstrating the SMC's response to the manual input and its ability to stabilize the roll despite the disturbance.
- Pitch: The pitch angle remains relatively stable during the roll direction change, indicating that the SMC effectively isolated the pitch control from the roll disturbance, maintaining the desired pitch angle.
 - Yaw: The yaw angle subplot shows the yaw response, with the SMC managing to keep yaw disturbances minimal during the roll adjustment, ensuring coordinated control of the aircraft's attitude.
- Servo flap positions (bottom-right):
 - Roll servo flaps: The roll servo positions indicate significant activity around minute 30, as the SMC adjusts the control surfaces to manage the changing roll direction. The servos' responses highlight the controller's ability to adapt to changing conditions swiftly.
 - Pitch servo flaps: The pitch servo positions show minimal deviation, reflecting the controller's focus on maintaining a stable pitch despite the roll inputs.
 - Yaw servo flaps: The yaw servo positions illustrate the minor adjustments made to maintain directional stability, complementing the roll and pitch control efforts.
- Altitude (top-left): The altitude plot shows the actual altitude (in red) and the desired altitude (in blue). At approximately minute 12, the altitude climbs sharply from 5 m to 60 m as the control mode switches from manual to automatic. Another notable change occurs around minute 35, where the altitude adjusts to around 30 m, showcasing the SMC's capacity to manage altitude transitions smoothly.
 - Throttle (top-right): The throttle input subplot highlights the controller's adjustments to accommodate the changes in altitude. During the transitions at minutes 12 and 35, the throttle increases correspondingly, demonstrating the controller's responsiveness to altitude commands and its ability to stabilize the helicopter.
 - Flight trajectory (center): The 3D flight trajectory plot illustrates the helicopter's path, emphasizing the altitude changes at the specified times. The plot shows a controlled ascent and descent, indicating the SMC's effectiveness in managing the transitions between different altitudes and control modes.
 - Roll, pitch, and yaw (bottom-left):
 - Roll: The roll angle plot indicates minor fluctuations during the altitude changes, with the SMC maintaining stability and closely following the desired roll angle.
 - Pitch: The pitch angle plot shows consistent control during the flight, with the pitch remaining stable even during the altitude transitions at minutes 12 and 35.
 - Yaw: The yaw angle subplot highlights the controller's ability to maintain directional stability during the altitude changes and control mode transitions, with minimal deviations from the desired yaw angle.
- Servo flap positions (bottom-right):
 - Roll servo flaps: The roll servo flap positions reflect the adjustments made by the SMC to stabilize the helicopter during the altitude transitions and control mode changes.
 - Pitch servo flaps: The pitch servo flap positions show the SMC's active management of pitch stability, particularly during the altitude changes, ensuring smooth control.
 - Yaw servo flaps: The yaw servo positions depict the control inputs made to maintain yaw stability, demonstrating the SMC's ability to handle directional changes effectively.

Overall the strength points of Figures 2–5 rather than Figure 6 could be highlighted as follows:

- Robust altitude control: The SMC shows excellent performance in maintaining the desired altitude, even with potential disturbances, demonstrating its reliability and robustness.
- Efficient throttle management: The throttle control is stable, ensuring efficient power usage and smooth altitude adjustments.
- Accurate trajectory following: The helicopter's flight path is well-managed, highlighting the controller's precision in following the intended trajectory.
- Stable attitude control: The roll, pitch, and yaw angles are maintained with high accuracy, contributing to the overall stability and safety of the helicopter.
- Responsive servo control: The servo flap positions indicate a responsive and precise control system capable of quick adjustments, essential for maintaining flight stability and performance.

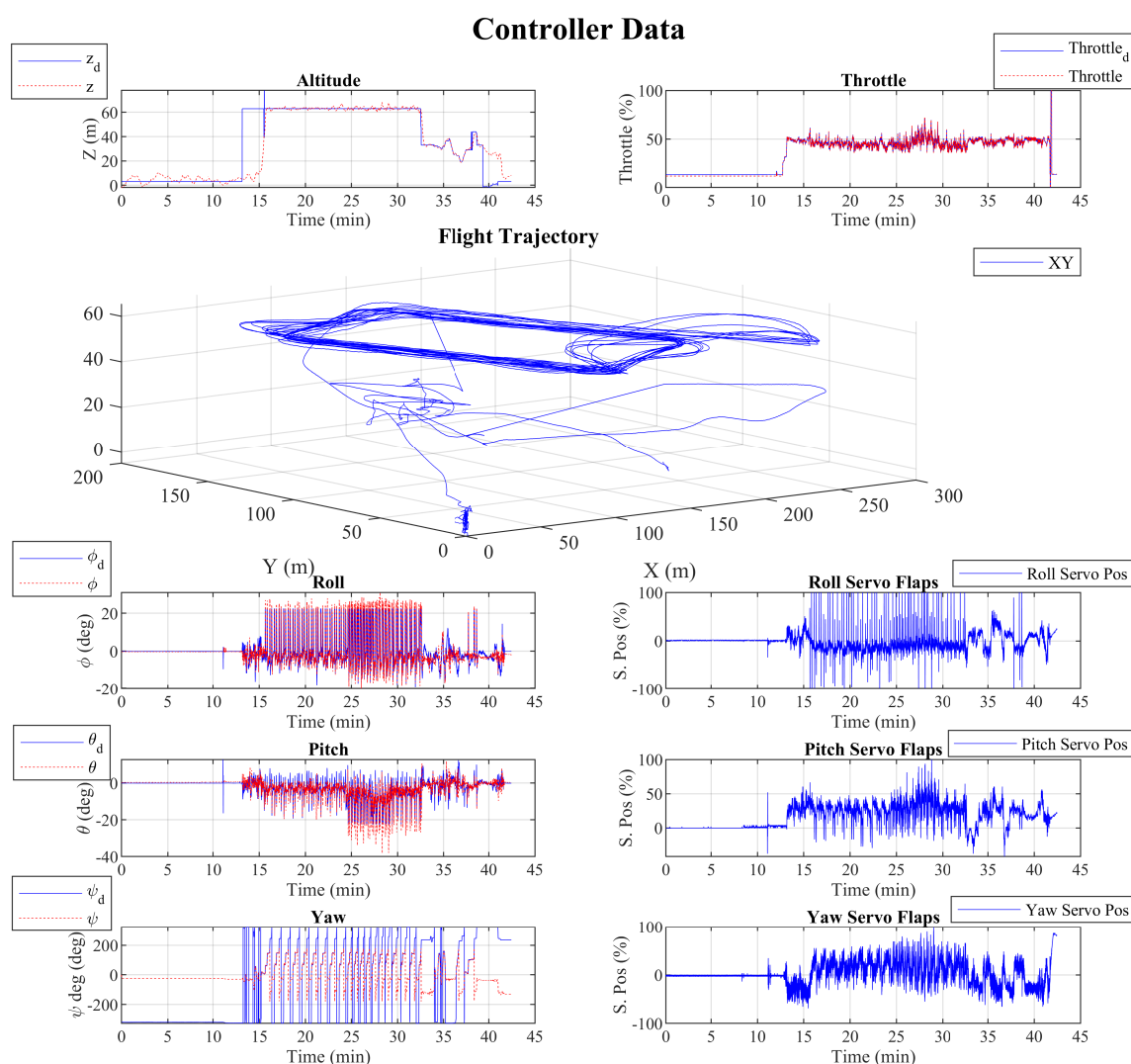


Figure 6. Performance data of the Nuntius helicopter controlled by a secured SMC during a 50-min flight. The flight includes transitions between manual and automatic control modes, with significant altitude changes at around minute 12 and minute 35. The figure evaluates the controller's performance in maintaining stability and handling these transitions.

4. Conclusions

This paper presents a robust sliding mode control (SMC) framework specifically tailored to enhance the security and resilience of unmanned aerial vehicles (UAVs) in challenging environments. The integration of adaptive and fault-tolerant mechanisms into

the SMC design ensures that the UAV maintains stability and performance even in the presence of disturbances, faults, and cyber-physical attacks. The successful implementation and simulation on a helicopter UAV platform, Nuntius-02, demonstrate the practical effectiveness of the proposed control strategy.

Simulation results show that the SMC-based control system effectively maintains the UAV's stability across various scenarios, including significant disturbances and simulated attacks. The adaptive mechanisms were particularly effective in dynamically adjusting control parameters in real time, thereby mitigating the effects of unexpected anomalies. Moreover, the fault-tolerant aspects of the control strategy ensured continued operation despite simulated component failures, with the UAV consistently following its intended flight path and maintaining the desired altitude and attitude. Also, the figures provided demonstrate the effectiveness of the SMC-based control framework in handling high-frequency disturbances: Figures 2 and 3 highlight the controller's performance when random noise is applied to the yaw angle, simulating high-frequency disturbances. The SMC maintained stability, with minimal deviations in key flight parameters. Figure 5 shows the helicopter's response to a sudden change in the roll direction. The controller effectively managed this disturbance, maintaining stable flight. Figures 4 and 6 illustrate the system's robustness during transitions between manual and automatic modes, including sharp altitude changes, demonstrating the SMC's ability to handle rapid disturbances. These results confirm the controller's robustness against high-frequency disturbances, ensuring stable UAV operation under challenging conditions.

Despite the advancements presented in this study, some limitations warrant further exploration. The reliance on simulation environments for testing the SMC-based framework may not fully capture the complexities and unpredictabilities of real-world UAV operations. Thus, experimental validation in real-world settings is necessary to confirm the robustness and effectiveness of the framework under diverse and dynamic conditions. Additionally, the study's focus on a specific UAV platform may limit the generalizability of the findings, suggesting a need to apply this framework across different UAV configurations. Future work could also expand the range of tested attack scenarios and incorporate more sophisticated anomaly-detection algorithms. Moreover, the development of hybrid control strategies, combining SMC with other advanced control techniques, could offer enhanced robustness and flexibility, paving the way for more secure and reliable UAV operations in increasingly complex and hostile environments.

Author Contributions: Conceptualization, M.S.A.I., P.F.P., D.G. and A.R.R.; methodology, M.S.A.I., P.F.P., D.G. and A.R.R.; software, M.S.A.I. and A.R.R.; validation, M.S.A.I., P.F.P., D.G. and A.R.R.; formal analysis, P.F.P. and A.R.R.; investigation, M.S.A.I. and D.G.; resources, P.F.P. and A.R.R.; data curation, M.S.A.I., P.F.P., D.G. and A.R.R.; writing—original draft preparation, M.S.A.I. and A.R.R.; writing—review and editing, M.S.A.I., P.F.P., D.G. and A.R.R.; visualization, M.S.A.I., P.F.P., D.G. and A.R.R.; supervision, D.G. and A.R.R.; project administration, P.F.P. and A.R.R.; funding acquisition, A.R.R. All authors have read and agreed to the published version of the manuscript.

Funding: This project has been funded by the European Commission under Grant Agreement Ref. 59/163630.9/23.

Data Availability Statement: The data presented in this study are available on request from the corresponding author.

Acknowledgments: We extend our heartfelt gratitude to the Community of Madrid for their support and funding of this research under the project “SOSTEVAL” [LA MEJORA DE LA COOPERACIÓN PÚBLICO PRIVADA EN MATERIA DE I + D + I MEDIANTE PROYECTOS DE EFECTO TRACTOR EN CONSORCIO, COFINANCIADAS POR EL FONDO EUROPEO DE DESARROLLO REGIONAL DENTRO DEL PROGRAMA OPERATIVO FEDER DE LA COMUNIDAD DE MADRID PARA EL PERÍODO 2021–2027]. We also thank Carlos III University for providing the necessary resources and academic environment to pursue this investigation.

Conflicts of Interest: The company was not involved in the actual research, and there is no conflict of interest.

References

1. Federal Aviation Administration. *FAA Aerospace Forecast FY 2023–2043*; Federal Aviation Administration: Washington, DC, USA, 2023.
2. Dasgupta, D.; Akhtar, Z.; Sen, S. Machine learning in cybersecurity: A comprehensive survey. *J. Def. Model. Simul.* **2022**, *19*, 57–106. [[CrossRef](#)]
3. Tsao, K.Y.; Girdler, T.; Vassilakis, V.G. A survey of cyber security threats and solutions for UAV communications and flying ad-hoc networks. *Ad. Hoc. Netw.* **2022**, *133*, 102894. [[CrossRef](#)]
4. Sihag, V.; Choudhary, G.; Choudhary, P.; Dragoni, N. Cyber4Drone: A Systematic Review of Cyber Security and Forensics in Next-Generation Drones. *Drones* **2023**, *7*, 430. [[CrossRef](#)]
5. Altawy, R.; Youssef, A.M. Security, Privacy, and Safety Aspects of Civilian Drones: A Survey. *ACM Trans. Cyber-Phys. Syst.* **2016**, *1*, 7. [[CrossRef](#)]
6. Krishna, C.L.; Murphy, R.R. A review on cybersecurity vulnerabilities for unmanned aerial vehicles. In Proceedings of the 2017 IEEE International Symposium on Safety, Security and Rescue Robotics (SSRR), Shanghai, China, 11–13 October 2017; IEEE: Piscataway, NJ, USA, 2017; pp. 194–199.
7. Hartmann, K.; Steup, C. The Vulnerability of UAVs to Cyber Attacks—An Approach to the Risk Assessment. In Proceedings of the 5th International Conference on Cyber Conflict, Tallinn, Estonia, 4–7 June 2013; Podins, K., Stinissen, J., Maybaum, M., Eds.; NATO CCD COE Publications: Tallinn, Estonia, 2013.
8. AL-Dosari, K.; Deif, A.M.; Kucukvar, M.; Onat, N.; Fetais, N. Security Supply Chain Using UAVs: Validation and Development of a UAV-Based Model for Qatar’s Mega Sporting Events. *Drones* **2023**, *7*, 555. [[CrossRef](#)]
9. Anagnostis, I.; Kotzanikolaou, P.; Douligeris, C. *Understanding and Securing Unmanned Aerial Vehicle (UAV) Services: A Comprehensive Tutorial*; Authorea Preprints: Hoboken, NJ, USA, 2024.
10. Mekdad, Y.; Aris, A.; Babun, L.; El Fergougui, A.; Conti, M.; Lazzeretti, R.; Uluagac, A.S. A survey on security and privacy issues of UAVs. *Comput. Netw.* **2023**, *224*, 109626. [[CrossRef](#)]
11. Fang, Z.; Savkin, A.V. Strategies for Optimized UAV Surveillance in Various Tasks and Scenarios: A Review. *Drones* **2024**, *8*, 193. [[CrossRef](#)]
12. Hadi, H.J.; Cao, Y.; Nisa, K.U.; Jamil, A.M.; Ni, Q. A comprehensive survey on security, privacy issues and emerging defence technologies for UAVs. *J. Netw. Comput. Appl.* **2023**, *213*, 103607. [[CrossRef](#)]
13. Tlili, F.; Ayed, S.; Fourati, L.C. Advancing UAV security with artificial intelligence: A comprehensive survey of techniques and future directions. *Internet Things* **2024**, *27*, 101281. [[CrossRef](#)]
14. Mykytyn, P.; Brzozowski, M.; Dyka, Z.; Langendoerfer, P. A Survey on Sensor-and Communication-Based Issues of Autonomous UAVs. *CMES-Comput. Model. Eng. Sci.* **2024**, *138*, 1019–1050. [[CrossRef](#)]
15. Kumar, N.; Chaudhary, A. Surveying cybersecurity vulnerabilities and countermeasures for enhancing UAV security. *Comput. Netw.* **2024**, *252*, 110695. [[CrossRef](#)]
16. Abro, G.E.M.; Zulkifli, S.A.B.M.; Masood, R.J.; Asirvadam, V.S.; Laouiti, A. Comprehensive Review of UAV Detection, Security, and Communication Advancements to Prevent Threats. *Drones* **2022**, *6*, 284. [[CrossRef](#)]
17. Yaacoub, J.P.; Noura, H.; Salman, O.; Chehab, A. Security analysis of drone systems: Attacks, limitations, and recommendations. *Internet Things* **2020**, *11*, 100218. [[CrossRef](#)]
18. Pandey, G.K.; Gurjar, D.S.; Nguyen, H.H.; Yadav, S. Security Threats and Mitigation Techniques in UAV Communications: A Comprehensive Survey. *IEEE Access* **2022**, *10*, 3215975. [[CrossRef](#)]
19. Shafik, W.; Matinkhah, S.M.; Shokoor, F. Cybersecurity in Unmanned Aerial Vehicles: A Review. *Int. J. Smart Sens. Intell. Syst.* **2023**, *16*. [[CrossRef](#)]
20. Gu, Y.; Guo, K.; Guo, L.; Qiao, J.; Jia, J.; Yu, X.; Xie, L. An Enhanced UAV Safety Control Scheme Against Attacks on Desired Trajectory. *Aerosp. Sci. Technol.* **2021**, *119*, 107212. [[CrossRef](#)]
21. Ale Isaac, M.S.; Luna, M.A.; Ragab, A.R.; Ale Eshagh Khoeini, M.M.; Kalra, R.; Campoy, P.; Flores Peña, P.; Molina, M. Medium-scale uavs: A practical control system considering aerodynamics analysis. *Drones* **2022**, *6*, 244. [[CrossRef](#)]
22. Isaac, M.S.A.; Ragab, A.R.; Garcés, E.C.; Luna, M.A.; Peña, P.F.; Cervera, P.C. Mathematical modeling and designing a heavy hybrid-electric quadcopter, controlled by flaps. *Unmanned Syst.* **2022**, *10*, 241–253. [[CrossRef](#)]
23. Ale Isaac, M.S.; Ragab, A.R.; Luna, M.A.; Ale Eshagh Khoeini, M.M.; Campoy, P. Thrust Vectoring Control for Heavy UAVs, Employing a Redundant Communication System. *Sensors* **2023**, *23*, 5561. [[CrossRef](#)]
24. Ale Isaac, M.S.; Flores Pena, P.; Andres Luna, M.; Refaat Ragab, A.; Campoy, P. Sensing and Control Integration for Thrust Vectoring in Heavy UAVs: Real-World Implementation and Performance Analysis. *Unmanned Syst.* **2024**, *1*–23. [[CrossRef](#)]
25. Yin, T.; Gu, Z.; Xie, X. Observer-Based Event-Triggered Sliding Mode Control for Secure Formation Tracking of Multi-UAV Systems. *IEEE Trans. Netw. Sci. Eng.* **2023**, *10*, 887–895. [[CrossRef](#)]
26. Xiao, J.; Feroskhan, M. Cyber Attack Detection and Isolation for a Quadrotor UAV With Modified Sliding Innovation Sequences. *IEEE Trans. Veh. Technol.* **2022**, *71*, 7202–7214. [[CrossRef](#)]
27. Liu, C.; Shaoshan, S.; Chenggang, T.; Shou, Y.; Xu, B. Sliding Mode Control of Multi-Agent System with Application to UAV Air Combat. *Comput. Electr. Eng.* **2021**, *96*, 107491. [[CrossRef](#)]
28. Bao, C.; Guo, Y.; Luo, L.; Su, G. Design of a Fixed-Wing UAV Controller Based on Adaptive Backstepping Sliding Mode Control Method. *IEEE Access* **2021**, *9*, 107491. [[CrossRef](#)]

29. Olguin-Roque, J.; Salazar, S.; González-Hernandez, I.; Lozano, R. A Robust Fixed-Time Sliding Mode Control for Quadrotor UAV. *Algorithms* **2023**, *16*, 229. [[CrossRef](#)]
30. Krishna, A.B.; Sen, A.; Kothari, M. Robust Geometric Control of a Helicopter using Sliding Mode Control. In Proceedings of the 2020 International Conference on Unmanned Aircraft Systems (ICUAS), Athens, Greece, 1–4 September 2020; pp. 737–743. [[CrossRef](#)]
31. Zhou, B.; Tang, S.; Li, P.; Zheng, Z. Sliding mode attitude controller design of a small-scale helicopter. In Proceedings of the 26th Chinese Control and Decision Conference (2014 CCDC), Changsha, China, 31 May–2 June 2014; pp. 2441–2446. [[CrossRef](#)]

Disclaimer/Publisher's Note: The statements, opinions and data contained in all publications are solely those of the individual author(s) and contributor(s) and not of MDPI and/or the editor(s). MDPI and/or the editor(s) disclaim responsibility for any injury to people or property resulting from any ideas, methods, instructions or products referred to in the content.